Parameters of Tomonaga-Luttinger liquid in a quasi-one-dimensional material with Coulomb interactions

Piotr Chudzinski

School of Mathematics and Physics, Queen's University of Belfast, BT7 1NN Belfast, Belfast, United Kingdom
and Institute of Fundamental Technological Research, Polish Academy of Science, Pawinskiego 5B, 02-106 Warszawa, Poland

(Received 20 February 2020; revised 3 October 2020; accepted 22 February 2021; published 13 April 2021)

We derive a scheme to calculate the Tomonaga-Luttinger liquid's (TLL) parameters and the holon velocity in a quasi-one-dimensional (quasi-1D) material that consists of two-leg ladders coupled through Coulomb interactions. First, we obtain an analytic formula for electron-electron interaction potential along the conducting axis for a generalized charge distribution in a plane perpendicular to it. Then, we introduce many-body screening that is present in a quasi-1D material by proposing an approximation for the charge susceptibility. Based on this we are able to find the TLL's parameters and velocities. We then show how to use these to validate the experimental angle-resolved photoemission spectroscopy data measured recently in p polarization in $NbSe_3$. Although we focus our study on this specific material, it is applicable for any quasi-1D system that consists of two-leg ladders as its basic units.

DOI: 10.1103/PhysRevB.103.155122

I. INTRODUCTION

A quasi-one-dimensional (quasi-1D) material can be imagined as a set of many conducting columns, where quantum coherent propagation is possible along each column but not in-between them. Such situation can be realized in a bundle of nanotubes, in a network of dislocation in topological insulator, but also in certain materials with a characteristic columnar structure. Since carriers cannot avoid each other in their motion, we expect that collective behavior will dominate, the metallic phase breaks the Fermi-liquid paradigm and becomes Tomonaga-Luttinger liquid, as first proposed by Haldane [1].

The most outstanding hallmark of a collective, non-Fermi-liquid behavior in 1D metals is the fact that spin and charge excitations propagate with different velocities. Probing this spin-charge separation in quasi-1D materials has been one of the long-standing [2] challenges in experimental solid-state physics of strongly correlated systems. Although the task of detecting two electronic dispersions sounds relatively simple, it is actually not so due to broadness of the peaks of the Tomonaga-Luttinger liquid (TLL) spectral function $A(q, \omega)$ and anomalously low intensity of some of them. These are generic, unavoidable properties of the collective TLL state [3,4]. To overcome these difficulties and produce an unambiguous proof of the spin-charge separation, most of the recent experimental evidences [5–7] are combined with a theoretical estimate of the expected ratio of the two velocities to obtain a quantitative agreement between the experiment and the theory. The situation on the theory side is, however, far from trivial. While there are many [8] numerical [9–11] and Bethe ansatz [12] methods and spectroscopy-matching procedures [6] for materials described by Hubbard-type models, with short-range interactions, only few theoretical studies are available for systems with long-range interactions. This is despite the fact that systems with long-range interactions are more frequently encountered in nature. Carbon nanotubes are one realization where, for the single-wall metallic achiral tubes, the analytical theory has been provided in a seminal work [13]. However, this works only for the specific class of highly symmetric systems. One of the key findings of our work is that the distribution of charge density within a cross section of the 1D column, in other words on the circumference of the tube, does affect the holon velocity. Actually, knowledge of this density is sufficient information to determine the holon velocity. This explains the importance of our aim: to derive a general theory applicable to systems where the charge distribution has a lower local symmetry. We provide analytical expressions for the desired quantities, which, contrary to numerical results, are easily transferable from one experimental realization to another.

We choose to study a model of two-leg ladders with long-range interactions. The underlying reason why the models with long-range interactions are more appropriate to describe (quasi-)1D materials is because 1D metals cannot screen long-range interactions. To be specific, let us consider a material with several occupied bands, where only one of them crosses, with strongly anisotropic dispersion, the Fermi energy, while all other orbitals are semiconducting as it is [14] in the case of $NbSe_3$ as well as other 1D materials e.g. $Li_{0.9}Mo_6O_{17}$ [15]. For example, this can be the t_{2g} manifold of d orbitals with d_{xz} electrons constituting an anisotropic metal while d_{xy}, d_{yz} play the role of "other" semiconducting orbitals. The model with short-range Hubbard UV interactions is valid for a quasi-1D material only when the "other" two-dimensional (2D) [or three-dimensional (3D)] bands can provide screening. Namely, to provide enough screening these other orbitals should fall sufficiently close (a fraction of a bandwidth) to the E_F. However, the opposite situation is more frequent,

where the other bands overlap (in energy) only with the very bottom of the 1D band. Then there is a broad energy window where the unscreened 1D metal exists. In this situation, the expressions derived in this work have to be used.

The reason why we decided to study two-leg ladders is related to underlying crystal-lattice effects. The simpler the 1D column is, the more likely it is that it will undergo the Peierls transition, effectively obscuring low-energy TLL behavior. Hence, our search for the TLL realization should move to slightly more complicated systems. The next simplest one is that where two Fermi points split in four making a complete nesting (commensurability) much harder to achieve. This is a two-leg ladder model for the 1D column, the subject of this study. From a theoretical perspective the price to pay is that the more complicated 1D column will most likely have lower internal symmetry, hence, a generalization of past works [13] is a necessity.

In an overwhelming majority of works on the 1D quantum liquids the TLL parameters, velocity, and compressibility of the modes are considered to be known input variables. It is usually assumed that the TLL parameters are extracted from numerics [8,9] (see, for example, [10,11]). The philosophy of this work is opposite: We aim to provide a close analytic formula for TLL parameters and then to confront this prediction with experimental results. In the past there were analytical works for two-leg ladders, but these were relying on an emergent SO(8) symmetry at the ultimate fixed point [16,17]. These high-symmetry point values will be measurable only at the lowest temperatures and frequencies when the emergent symmetry settles, which in case of long-range interactions may fall at a fraction [13] of mK, while in the frequency and temperature range realistically accessible in angle-resolved photoemission spectroscopy (ARPES) experiments [3] one is always probing a system with lower symmetry. This is the reason why it is also worthwhile to provide the theory for the lower-symmetry system and why here we aim for analytical formulas for such a case.

The model that we propose is indeed sufficient to allow for an experimental observation of TLL phase. Our study is motivated by a recent experimental report [18,19] of 1D TLL states observed in p polarization in $NbSe_3$. We can summarize those findings as follows: (i) At each Fermi point there are *two* linear dispersions [19], at the inner band (following Ref. [18] we shall call this antibonding band $A1$, hence the Fermi point k_{F1}) the two velocities converge to the same value, at outer band $A3$ the two velocities are different (one $A3_s$ is equal to those at k_{F1} while the other $A3_h$ is a factor $\approx$1.25 larger). (ii) The spectral function can be fitted with a finite-temperature expression [20] for the TLL $A(\omega, T)$ with the characteristic Green's function exponent [19] $\alpha = 0.24$. It is surprising that with such a small ratio of velocities there is such a substantial value of α exponent, and our aim here is to explain this experimental finding.

The paper is organized as follows. We start in Sec. II by introducing carefully the multimode TLL Hamiltonian and its applicability. Then, in Sec. III we derive the Coulomb interaction's potential along the 1D column (along crystal b axis) without assuming that its charge density has a perfect cylindrical. With this, in Sec. IV, we tackle the system of several weakly coupled columns with a partial screening incorporated in the solution: we provide analytical formula for screening (Sec. IV A) and then the TLL parameters for the entire quasi-1D material (Sec. IV B). Then, we focus on the measurable quantities in a concrete realization $NbSe_3$: we compute the value of the ratio between holon to other mode velocities and the single-particle spectral function exponent (Sec. V) and derive Coulomb-potential selection rules that govern relative intensities of various modes (Sec. VI). Then, we can analyze the result of the ARPES experiment [18,19]. The paper is completed with discussion and conclusions in Sec. VII.

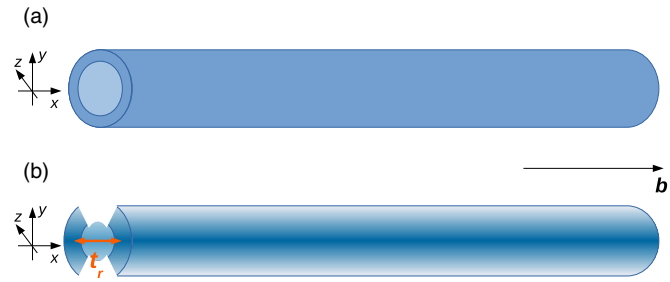

FIG. 1. Electronic (charge and spin) densities along a 1D column. (a) Homogeneous density on a surface of a cylinder, a tube. This is the case realized in, e.g., carbon nanotube and has been solved in Ref. [13]. (b) The case of more complex orbital when electrons reside only on a section of a tube, moreover with a density that is not uniformly distributed inside the occupied zone. In the case (b) we can define two parts connected through their respective orbital's hybridization t_r. In both cases, the 1D column is along the b axis of a quasi-1D crystal. Moreover, we define a local system of coordinates (x, y, z) which is used to integrate the interaction potential. Please note that in both cases we give a density that comes from an electron wave function in a given conduction band (eigenorbital) $\psi_{L/R,\alpha}(\vec{r})$ in a vicinity of the Fermi level.

II. TOMONAGA-LUTTINGER LIQUID

Consider a quasi-1D system consisting out of 1D units with coherent motion of electrons only along one direction, say x coordinate (or crystal b axis), and incoherent propagation in the perpendicular plane. Examples of such a single column are provided in Fig. 1 where an electronic density distribution is shown. As mentioned in the Introduction, these 1D units are sparse enough, so that screening is weak and interactions retain their Coulomb character. The theory that we develop here is valid for any 1D unit where the underlying, noninteracting fermionic theory has a dispersion with four Fermi points. This captures a broad class of materials: various tight-binding models of ladder-type materials but also bundles of nanotubes (based on carbon, but also silicon, tin, or bismuth) and stepped semiconductor surfaces, e.g., silicon surface with gold atoms. In all these cases the effective theory is that of the Tomonaga-Luttinger liquid and what is relevant is the distribution of electronic cloud density that, as we show below, determines compressibility of the collective 1D electronic liquid.

The low-energy properties of such material are determined by fluctuations around the four Fermi points. We aim for an effective low-energy theory of the 1D fermions. We use

quantum Grassmann field $\psi_{L/R,\alpha}(\vec{r})=\Psi_{L/R,\alpha}(\vec{r})\exp i[\phi_\nu(x)\pm\theta_\nu(x)]$ to describe them with the α index for instance for spin and bonding and antibonding band. The $\Psi_{L/R,\alpha}(\vec{r})=\exp(\pm ik_{F\alpha}x)\bar{\Psi}_\alpha(\vec{r})$ is a Bloch-type wave function enveloped with the high-energy atomistic wave function (in our convention the last one also contains the Klein factor). The low-energy physics is captured by slow fluctuations of the bosonic collective modes $\phi_\nu(x)$and $\theta_\nu(x)$. The Hamiltonian of the TLL state is written in terms of fluctuations of the low-energy collective bosonic modes:

$$H^{1D}[\nu]=\sum_\nu\int\frac{dx}{2\pi}\left[(v_\nu K_\nu)(\pi\Pi_\nu)^2+\left(\frac{v_\nu}{K_\nu}\right)(\partial_x\phi_\nu)^2\right], \tag{1}$$

where $x\parallel b$, $\nabla\phi_\nu(x)$ gives the local density of fluctuation of the νth mode $n_\nu(x)=\sum_\alpha c^\dagger_\alpha(x)\hat{v}c_{\alpha'}(x)$. The ν index can be spin/charge, total/transverse, while $\hat{v}$ is a corresponding operator which acts in α-space basis. For instance, if we start with a density functional theory (DFT) result and initially define states (and densities) in the band basis (so α is band+spin index) then $\hat{v}$ is a Pauli matrix $\hat{v}_0$ or $\hat{v}_z$ (total or transverse component) acting either on the band space or the spin space or on both. The v_ν, K_ν are velocity and TLL parameter ($\sim$compressibility) of a given bosonic mode ν, these depend on electron-electron interactions with small momentum exchange that is small momentum component of $V(r)$ in Eq. (2). In the simplest approximation $K_{c+}\approx(1-2g)$ where $g=V(q=0)/V_F$ is a strength of the electron-electron Coulomb interaction $q\to 0$. Assuming that Galilean invariance holds, the relation $v_\nu K_\nu=V_F$ is obeyed and gives us the v_ν. One immediately realizes that pure Coulomb interactions diverge when $q\to 0$ which makes g an ill-defined quantity. In this paper we shall improve this simple, approximate formula for v_ν.

Please note that the Hamiltonian above is for the pure TLL, with the backscattering cosine terms neglected. These latter terms would turn the model into sine-Gordon problem. Our assumption here is that the analytically solvable TLL theory applies as long as we are at energy (frequency and temperature) scale that is larger than the spectral gaps induced by these perturbing terms. In the case of Coulomb interactions $V(q\approx 0)\gg V(q\approx 2_{kF})$ so this assumption is reasonable. Below we show (detail discussion in Sec. VII B) that this assumption remains valid also in our more general model with lower symmetry of electronic cloud and a partial screening included.

The advantage of starting our derivation with Eq. (1) is that it captures the most general situation where our reasoning applies. To be specific, and to build a connection with $NbSe_3$, we shall now move to the ladder-type material, a system that is built out of 1D conducting columns, where each 1D column (along crystal b axis) consists of two identical strongly hybridized subunits. We see an example of this kind on the bottom panel in Fig. 1: the electronic density is split in two parts (left and right) with a density severely depleted on the top and bottom parts of the cylinder. Microscopically, this corresponds to some underlying arrangement of atoms and overlaps of their orbitals (see, e.g., Fig. 17 in Ref. [18] for an example of such a distribution in $NbSe_3$). However, for the purpose of this work, when we are interested in low-energy, long-wavelength properties, the only thing that matters is how in average the electronic density is spread for carriers on the conducting band. Hence, the schematic picture in Fig. 1 is sufficient.

When hybridization t_r of the two sides in Fig. 1(b) is strong enough, this leads to bonding and antibonding combinations of orbitals (bonds) through the column's center, hence, there are two bands crossing Fermi energy (example of such band structure is in Fig. 4 inset) and the two-leg ladder description indeed applies. An example of the simplest tight-binding Hamiltonian for such system is given in Appendix B, Eq. (B1). The coupling on rung t_r is assumed to be of the same order as the coupling along the leg of the ladder t_b and so it is *incorporated* into the single-particle band structure on the top of which the bosonization is defined. This is contrary to models where the t_r is considered perturbatively *after* bosonization; the in-depth discussion of the difference between these two classes of ladders is given in Ref. [21], while the transition from one case to another (the commensurate-incommensurate transition) has been solved in Ref. [22]. It is quite easy to see which case is realized: since the split of the two bands, e.g., bonding and antibonding one in the Fig. 4 inset, is proportional to t_r, then one can immediately diagnose which bosonization scheme applies in a given case. In our situation, with nonperturbative t_r, the four bosonic modes $\rho\pm$, $\sigma\pm$ now describe the cases where spin or charge oscillate symmetrically or antisymmetrically within the two legs of the ladder, which explains why we call them later total and transverse modes, respectively. The Fermi velocity V_F is $\sim 2t_b$ (if we take tight-binding model with 1D chains arranged along the b axis), this also determines the UV cutoff of our theory $2t_b\sim\Lambda_{UV}$.

III. SINGLE LADDER

The first step, in a quantitative treatment of Coulomb interactions, is to find their dependence as a function of inter-carriers' distance along the 1D column. The assumption is that we build our reasoning on the top of some single-particle DFT calculations, which presumably provides us with electronic density of the carriers occupying the 1D conduction band $\bar{\rho}_\alpha(\vec{r})=\bar{\Psi}^*_\alpha(\vec{r})\bar{\Psi}_\alpha(\vec{r})$. What such calculations are unable to capture are electron-electron correlations inevitably present in the 1D many-body state described by Eq. (1). We seek a way to determine v_ν, K_ν from the knowledge of single-particle physics. In our QFT, the Hamiltonian for electron-electron interaction reads as

$$H_{\rm int}=\int dx\,dx'\psi^\dagger_\alpha(\vec{r})\psi^\dagger_\beta(\vec{r}')\hat{V}(\hat{r}-r')\psi_\gamma(\vec{r})\psi_\delta(\vec{r}'), \tag{2}$$

where $\alpha,\beta,\gamma,\delta$ contain spin and band indices of the fermionic field. Using standard second quantization prescription the kernel is given by a bra-ket: $V^{\gamma\delta}_{\alpha\beta}(|\vec{r}-\vec{r'}|)=\langle\vec{r}\alpha,\vec{r}'\beta|\hat{V}(\hat{r}-\hat{r}')|\vec{r}\gamma,\vec{r}'\delta\rangle$. Since we are interested only in the long-distance component along the 1D system the scattering amplitude (that enters to second quantization Hamiltonian) of

the Hartree type $\alpha = \gamma$, $\beta = \delta$ interaction is given by

$$V_{\alpha\beta}(x-x')|_{(x-x')>a} = \int_{UC} d\vec{r}_\perp d\vec{r}'_\perp \Psi^*_\alpha(\vec{r})\Psi^*_\beta(\vec{r}') \times \bar{V}_{\rm Coul}(\vec{r}-\vec{r}')\Psi_\alpha(\vec{r})\Psi_\beta(\vec{r}'). \quad (3)$$

Here, an integral is over the unit cell, i.e., the perpendicular coordinates $\vec{r}_\perp = (y, z)$ of *one* 1D column. Since we are interested in a long-distance (effective low-energy) theory the fluctuations along the x coordinate are either assumed to be already averaged out or are integrated out (from zero distance up to length $a \sim \Lambda_{\rm UV}^{-1}$) at this step. The bare Coulomb potential for a 1D column of charge density can be expressed as follows [13]:

$$\bar{V}_{\rm Coul}(\vec{r}-\vec{r}') = \frac{e^2/\kappa}{\sqrt{(x-x')^2 + 4R^2\sin^2[(y-y')/2R] + d^2}}, \quad (4)$$

where the d is a thickness of the charge layer, R is an average radius of the 1D column, and κ is an effective dielectric constant chosen to give a desired $\bar{U}$ in Eq. (6). The dependence on $\vec{r} = [x, y]$ is set in the same way as in Ref. [13] (with the perpendicular coordinate y as one cathetus and R a hypotenuse of the right-angled triangle). For a carbon nanotube with homogeneous (angle-independent) charge distribution, the integration over perpendicular coordinate (angle) would result in elliptic integral of the first kind [13]. However, we pertain to capture more complex geometry. The difference is shown in Fig. 1 where on the top panel we show the homogeneous nanotube case that has been solved in Ref. [13] while on the bottom is our system which enables to model situation where atoms of different type are located in a less symmetric arrangement (see, e.g., Fig. 17 in Ref. [18] for the specific $NbSe_3$ configuration). The charge density can now be spread only over a finite angle ϕ_α sector of a distorted hollow cylinder. Examples of its cross sections are in Fig. 4. We add an extra parameter ζ that accounts for an inhomogeneity along the circumference where $\zeta = 0$ correspond to the symmetric homogeneous distribution (and a constant radius) like in nanotube. Hence, we generalize the expression given in Ref. [13] with symmetry reduced from $C_\infty(\vec{b})$ down to $C_4(\vec{b})$, $S_4(\vec{b})$. We integrate over perpendicular coordinates[1] to get an interaction amplitude along the b axis $V(x)$:

$$V_{\alpha\beta}(x-x') = \int_{\phi_\alpha R}^{2\pi R}\int_{\phi_\beta R}^{2\pi R} \frac{dy}{2\pi R}\frac{dy'}{2\pi R}\frac{\bar{V}_{\rm Coul}(\vec{r}-\vec{r}')}{1-\zeta\sin[(y-y')/2R]}, \quad (5)$$

where $\zeta = \sqrt{\zeta_\alpha\zeta_\beta}$. The closed analytic form for the integral is known also in this more general case:

$$V(x-x') = \bar{U}\frac{\sqrt{1-\zeta^2}\,\Pi\left(\phi;\zeta\middle|\left(\frac{2R}{\sqrt{d^2+4R^2+(x-x')^2}}\right)^2\right)}{\left(\phi\sqrt{d^2+4R^2+(x-x')^2}\right)}, \quad (6)$$

where $\Pi(\phi;\zeta|1/\tilde{x})$ is the incomplete elliptic integral of the third kind. The integral is parametrized by $\bar{U} = U/N$ [$\bar{U} \equiv V^{\alpha\beta}_{\alpha\beta}(r=a)$ chosen appropriately depending on the *ab initio* method], e.g., for constrained random phase approximation (cRPA) we account for all screening provided by carriers residing on all other orbitals but not the 1D d orbital which is equivalent to saying that at a given UV cutoff Λ (usually proportional to the inverse lattice spacing) the correlation interactions saturate to a value given by local Hubbard-type repulsion. The parameters ϕ (angle of the sector of the toroid) and ζ (distortion of the toroid) are determined by the geometry of the given *eigenorbital* in the a-c plane perpendicular to 1D axis. The prefactor ensures that no matter what the geometry is, there total density of charge is normalized. We need to perform Fourier transform of $V(x)$; this will complete our description of the Hartree term in a single ladder and column, and the result is illustrated in Fig. 2.

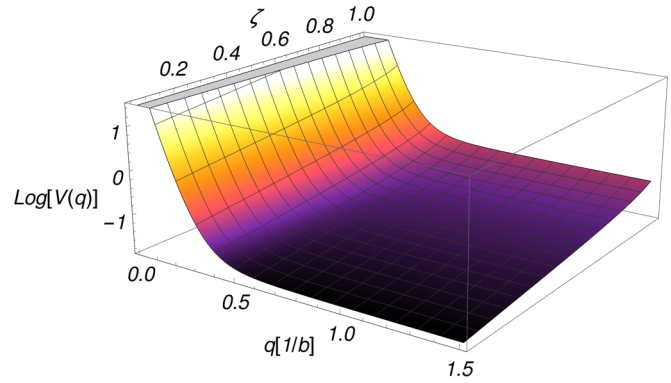

FIG. 2. Fourier transform of the Coulomb interaction (6) shown as a function of momentum and parameter ζ that describes inhomogeneity (eccentricity) of the $\rho(\vec{r})$ cross section.

For Coulomb electron-electron interactions there shall be also exchange interactions $\alpha = \delta, \beta = \gamma$ in Eq. (2). Their value for $r = a$ is again known from the *ab initio* calculations

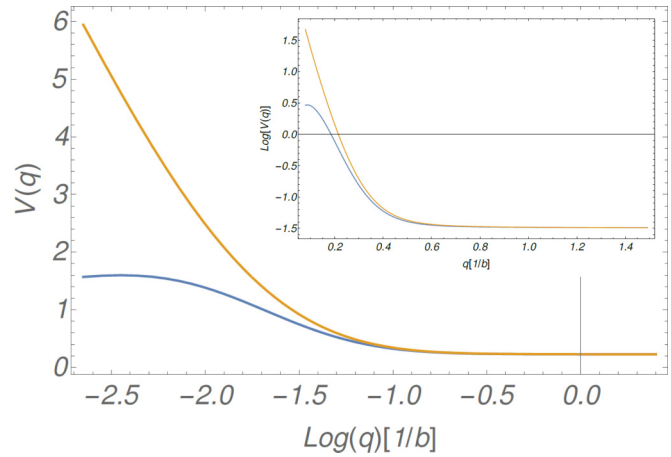

FIG. 3. Screening effects in quasi-1D material. Logarithm of electron-electron interactions as a function of momentum q is shown. The yellow curve is for bare nonscreened $V_{\rm Coul}(q)$, a Fourier transform of Eq. (6), while the blue line is screened by the susceptibility given in Eq. (7). The main plot is in log-linear coordinates and manifest the asymptotic $\sim \log(q)$ behavior while the inset is in linear-log coordinates to show the real momentum dependence.

[1]Here the integral over short distance $x < a$ is trivial as it is in essence a convolution by a Dirac delta. However, this integration will turn out to be nontrivial for exchange term below.

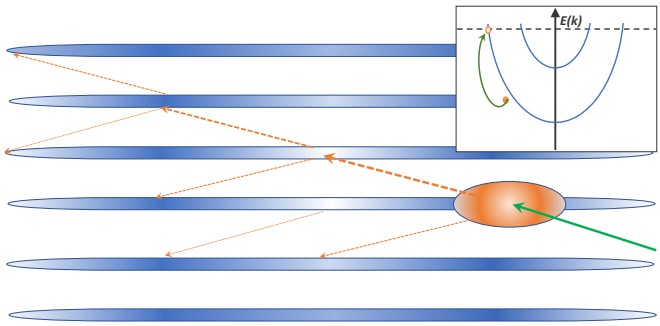

FIG. 4. An ARPES photoemission event shown in the real space. We see that a photon (green arrow) incoming with a finite $q_\perp$ shall induce charge density fluctuations not only in the 1D ladder where photohole (orange oval) has been instantaneously created, but (through screened Coulomb interactions, orange arrows) in the surrounding 1D systems. An inset shows the same event in a reciprocal space: instantaneous recombination of a photohole with a fermion at one of the Fermi points (together we call this object a photodensity).

and parametrized by $V^{\alpha\beta}_{\beta\alpha}(r=a)=J$. For a system with long-range interactions, this can be thought of as an interaction of a carrier with an exchange hole of another carrier. The exchange hole is described by a two-body correlation function $g(x,x')$. This extra term will convolve one of the wave functions $\Psi_\alpha(x')$ in Eq. (3). The two-body density, in a translationally invariant TLL, has a dominant contribution that scales like $g(x')\sim(x')^{-[1/4(1/K_{\rho+}+3/K_s)+2]}$ for large x, where in our case $K_s=1$. For a sufficiently strong repulsive interaction $K_{\rho+}\ll 1$, we convolve Eq. (3) with the function $g(x)$ that rapidly decays in real space which agrees well with our intuitive understanding of exchange. Then, the overall Fourier transform $J(q)=F[V(x)\otimes g(x)](q)$ will be the previous Fourier transform of screened Coulomb potential $V(q)$ times an increasing power law $F[g(x)](q)$. As a result, the $J(q=2k_F)$ may be non-negligible. Please note that the $J(q=2k_F)$ enters only to g_2 term in TLL language while it does not enter to backscattering terms $g_1\sim J(q=0)$.

IV. QUASI-1D MATERIAL

A. Screening

A fundamental problem with the Fourier transform of Eq. (6) is that in the limit $q\to 0$ it diverges and we find that changing the parameters of electronic density (ζ,ϕ,R,d) in Eq. (6) is not sufficient to fix this problem. Since $g=V(q\to 0)$, then this implies that TLL parameters are undefined. A standard way to overcome this problem has been to assume a mesoscopic realization, with some finite charging energy, which is equivalent of imposing an arbitrary IR cutoff. Here, we shall proceed in a different way, by considering a screening in a realistic 3D material, a quasi-1D material, i.e., a system that consists of multitude of parallel ladders. This is shown in Fig. 4 where the 1D columns (each column is a ladder system) are indicated as a set of parallel blue rods.

Here, the full modeling has to account for the fact that we are dealing with a set of 1D systems coupled by long-range density-density (forward scattering) interactions; these interladder (charge) density-density terms are non-negligible, actually they can be as large as [23] $t_b/2$. We first compute screening of a single TLL by other columns which is sufficient to cut the divergence of $V(q)$ when $q\to 0$. To this end we take $V_{\rm eff}(q)=V(q)/[1+G(q,T)\chi_{\rm TLL}(q)]$. Here, we take an RPA approximation for the dielectric function. For the charge susceptibility of the two-leg ladder $\chi_{\rm TLL}(q)$ with one of the velocities $v_{\rho+}$ much different than V_F and all other velocities $v_{\rho-,\sigma\pm}\approx V_F$ (see below) and $K_{\rho-,\sigma\pm}\approx 1$ we can generalize the result obtained in Ref. [24]:

$$\chi_{\rm TLL}(q)=4\pi\frac{\Gamma\left[1-\left(\frac{K_{\rho+}}{4}+\frac{3}{8}\right)\right]}{\Gamma\left(\frac{K_{\rho+}}{4}+\frac{3}{8}\right)}\frac{|\omega^2-V_F^2q^2|^{\left(\frac{K_{\rho+}}{4}+\frac{3}{8}\right)-1}}{V_F^{\left(\frac{K_{\rho+}}{2}+\frac{3}{4}\right)-1}}\exp\left\{-\imath\pi\left[\left(\frac{K_{\rho+}}{4}+\frac{3}{8}\right)-1\right]\mathfrak{H}_\Theta\left[\omega^2-V_F^2q^2\right]\right\}$$
$$\times F_1\left(\frac{K_{\rho+}}{4},\frac{K_{\rho+}}{4}+\frac{3}{8}-\frac{1}{2},1-\left(\frac{K_{\rho+}}{4}+\frac{3}{8}\right),\frac{K_{\rho+}}{4}+\frac{3}{8};1-\left(\frac{v_{\rho+}}{V_F}\right)^2,1-\frac{\omega^2-v_{\rho+}^2q^2}{\omega^2-v_F^2q^2}\right)|_{\omega\to\Lambda^{\rm IR}},\qquad(7)$$

where $F_1(\ldots)$ is the Appell hypergeometric function and $\mathfrak{H}_\Theta$ is a Heaviside theta function that appears upon analytic continuation. Since we are interested in the smallest q and static response we work within the radius of convergence of the Appell hypergeometric function. For the $G(q,T)$, which accounts for a local field corrections we take $G(q,T)=\bar{G}(q,T)/(q^2+\Lambda_{\rm IR}^2)$. It is a screened Coulomb interaction times the static structure factor, the lesser correlation function of the screening medium, hence, by definition, what the local field correction is supposed to capture. We take $\bar{G}(q,T)\sim A(q,\omega\to 0,T;\Delta\equiv\Lambda_{\rm IR})$ where the spectral function is known from Ref. [25] and the IR cutoff $\Lambda_{\rm IR}=\max(T,t_\perp)$. With this choice the entire $G(q,T)$ can be interpreted as a propagator (i.e., a retarded correlation function in the Lehmann representation) of the bosons (the holons) carrying interactions in-between the 1D wires. Indeed, a sole 1D ladder cannot self-screen itself (and RPA expression is exact therein, local field corrections are absent) so the entire local field correction must originate from its environment. This approach, based on the $t_\perp$ tunneling, is sufficient to limit the increase of $V_{\rm eff}(q\to 0)$ to a well-defined constant value, which among other implications also gives a finite, nondivergent holon's velocity.

Although in Fig. 3 we show a quasi-1D material, our model of screening presented here applies also for bundles of nanotubes, rows of dislocations in 3D strong topological

insulators (TI), or networks of domain walls in 2D TI, basically is every situation where we can define an average $t_\perp$ and its variation is not large. Detail description of a problem of $t_\perp$ can be found in Ref. [26].

B. TLL parameters K_ν

The bosonization transformation $\psi_\alpha \to \phi_\nu, \theta_\nu$ is initially performed within $0/\pi$ bands so one begins with Hartree and Fock intraband and interband interactions. In each band we have Hartree $V(q)$ and Fock $J(q)$ and then it is known [27] that

$$\begin{aligned} g_{4mn} &= 1/2[2V_{(mn)}(q=0) - J_{(mn)}(q=0)]/\sqrt{V_{Fm}V_{Fn}}, \\ g_{2mn} &= ([V_{(mn)}(q=0) + J_{(mn)}(q=2k_{Fo/\pi})], \\ &\quad - 1/2[V_{(mn)}(q=2k_{Fo/\pi}) + J_{(mn)}(q=0)]/\sqrt{V_{Fm}V_{Fn}}, \\ g_{\sigma mn} &= -J_{(mn)}(q=0)/\sqrt{V_{Fm}V_{Fn}}, \end{aligned} \tag{8}$$

where $m, n = o, \pi$ [the α has been $\alpha = (o/\pi, \updownarrow)$] and we use notation of Ref. [27] for charge-current and spin-current processes. We took into account a possibility of different Fermi velocities in both bands, but we assumed that interaction terms do not depend on spin [otherwise, we would have had extra terms, e.g., $g_{\sigma oo} = V_{\uparrow,o}(0) - V_{\uparrow,\pi}(0)$]. The band dependence of interaction comes from their different shapes (see Appendix A for a detail discussion of the specific case of $NbSe_3$). Once the interactions are determined in a band basis one performs $S[\pi/4]$ rotation [28] to the total-transverse basis g_ν. For the neutral, chargeless modes $\rho-, \sigma\pm$ the interactions g_ν turn out to be small and we can use perturbation theory result. The TLL parameters and velocities for these three modes can be given by the following, single-ladder, formula: $K_\nu = \sqrt{\frac{1-g_{2\nu}-g_{4\nu}}{1+g_{2\nu}-g_{4\nu}}}$ where $g_{2\rho-} = (g_{2o} + g_{2\pi})/2 - g_{2o\pi}$, $g_{4\rho-} = (g_{4o} + g_{4\pi})/2 - g_{4o\pi}$, $g_{\sigma+} = g_{\sigma o} + g_{\sigma\pi}$, and $g_{\sigma-} = g_{\sigma o} - g_{\sigma\pi}$. We see that any interaction asymmetry of the two bands has an effect of pushing $K_{\rho-}$ away from 1. This can indeed happen in our more generalized system of distorted toroids, with distinct ζ, ϕ, R, d for the two bands, to be precise in most models we expect (see Appendix A) $K_{\rho-} < 1$. We can also deduce that with a physically reasonable interactions it will be the most difficult to move away from the $K_{\sigma-} = 1$ point.

In the bosonic language when interactions are spin or orbital independent at $q \to 0$ only the $\nabla\phi_{\rho+}$ operator is coupled with the long-range interactions, i.e., $g_{oo} \approx g_{\pi\pi} \approx g_{o\pi}$ implies that $g_{\rho+}$ is by far the largest. However, the quantity $v_{\rho+}$, the holon's velocity, that is experimentally measured is further modified by inter-chain interactions as we discuss separately in the following section. Here, it is worth mentioning that the results given here are valid also for multileg ladders, hence for a multimode TLL, with a Coulomb interactions provided that its symmetry (namely, existence of the mirror plane in Fig. 5) allows to separate out the total charge mode as the only one that is strongly coupled through Coulomb interactions.

V. HOLON MODE: CONNECTION WITH EXPERIMENT

Now we account for a finite aperture size in the ARPES experiment, which we intend to use as a test of our theory.

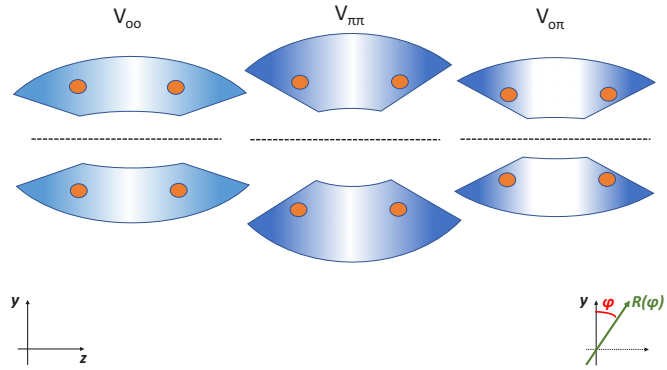

FIG. 5. Cross sections (in a-c plane) of three different types of 1D columns. The column was shown in Fig. 1(b). The intensity of blue shading corresponds to product of charge densities $\bar{\rho}_\alpha(\vec{r}_\perp)$ appearing in the integrand in Eq. (3). We have chosen, as an example, specific charge distributions corresponding to electronic states in $NbSe_3$ shown in Fig. 17 in Ref. [18]. We use these simplified pictures to obtain Hartree V_{mn} interactions in $NbSe_3$ in Sec. IV B. The three panels are for different orbital configurations, from left to right: $V_{oo} \sim \bar{\rho}_o(y,z)\bar{\rho}_o(y,z)$, $V_{\pi\pi} \sim \bar{\rho}_\pi(y,z)\bar{\rho}_\pi(y,z)$, $V_{o\pi}\bar{\rho}_o(y,z)\bar{\rho}_\pi(y,z)$. The horizontal black lines indicate a mirror plane symmetry that goes along the b axis and through the middle of the unit cell. The orange dots show approximate position of niobium atoms: the core of each trigonal biprismatic column [the entire 1D charge density shown in Fig. 1(b) consists out of four such entities]. We observe that radius R as well as distortion ζ and angular section ϕ are changing from one case to another. On the bottom left we show (y, z) local coordinates of the cross section, while on the bottom right are the variables that we use to perform an integral to get Eq. (6).

The finite aperture implies that the final state is a mixture of waves with different $q_\perp$ [this is a coherent state that results from Fresnel diffraction of electronic waves [26] (see Fig. 4)]. The problem is simplified because again only $\rho+$ modes are exposed to these long-range interactions. The treatment of this system can then be based directly on the solution provided by Schulz in Ref. [29]. In that work it was found that the velocity is equal to

$$v_{\rho+} = \frac{1}{\Delta q_\perp}\int_0^{\Delta q_\perp} dq_\perp V_F \sqrt{(1+g_{\rho+}^{(tot)})(1+2g_{4\rho+}-2g_{2\rho+})}, \tag{9}$$

where $g_{4\rho+} = \sum g_{4mn}$, $g_{\rho+}^{tot} = 2g_{4\rho+} + 2g_{2\rho+} + \tilde{g}_\perp$ with[2] $\tilde{g}_\perp = \frac{g_\perp}{\epsilon_\parallel^{(0)}(1+\epsilon_\perp^{(0)}(q_\parallel/q_\perp)^2}$. We take an integral over a finite $\Delta q_\perp$ in order to account for the finite aperture of the (Fresnel zone focused) nanoARPES device in Ref. [18], here we take [30] $\Delta q_\perp = \pi/6$. At the same time, the exponent of the single-particle Green's function (momentum integrated) is equal to $\alpha = (C_{\rho+} + C_{\rho+}^{-1})/8 + 6/8 - 1$ where $6/8$ comes from the three bosonic modes with $K_\nu \approx 1$ and

$$C_{\rho+} = \sqrt{\frac{1+2g_{4\rho+}-2g_{2\rho+}}{1+2g_{4\rho+}+2g_{2\rho+}}}\left(1 + \frac{\pi}{8}y_\perp \ln\left[\frac{y_\perp}{4}\right]\right), \tag{10}$$

[2]Here we profit from our treatment of V_{eff} and based on result in Fig. 3 we take $\epsilon_{\parallel,\perp}(q_\parallel) \sim (q_\parallel^2 + m^2)^{-1}$ which is equivalent to a model with an infinitesimally small many-body gap m.

where $y_\perp = \frac{g_\perp}{1+2g_{4\rho+}+2g_{2\rho+}}$The above formulas, with a physically sensible $g_\perp \in (0.4, 0.6)$, give the following estimates for observable quantities $v_{\rho+} \in (1.2, 1.35)V_F$ and $\alpha \in (0.15, 0.2)$.

VI. RELATIVE INTENSITY OF THE FOUR MODES

For the two-leg ladder with four TLL modes one expects four linear dispersions that start at each Fermi point. Below we show that in a realistic setting the intensity of half of these modes is strongly suppressed. The problem of a relation between theory and experimentally measured intensities is not new; its importance has been underlined, e.g., in Ref. [31]. The formula in Eq. (6) allows us not only to compute the parameters of the stationary TLL, but also to study the dynamics of an excited photohole. This in turn gives an insight into relative intensities measured for various TLL modes. To investigate the relative intensities of the four bosonic dispersions we take the two-step model for photoemission. In the first step, just after the photoemission event, the photohole (a single-fermion state) is created in an intermediate state $\psi_i(\vec{r})$ that is not an eigenstate but a localized combination of many excited states of the system. The $\psi_i(\vec{r})$ is located on atomic orbitals that fulfill *dipole matrix ARPES selection rules* and among these has to have a spatial distribution matching the evanescent wave of the emitted photoelectron, to ensure their large overlap. The photoelectron wave function can be computed by inverse scattering method [26] and from this calculation we know that $\psi_i(r_\perp) \approx H_0(r_\perp)$ inside the 1D column (that acts as a trap) where H_0 is the lowest-order Hermite polynomial. In the second step this initial excitation relaxes into the collective, bosonic TLL eigenstates of the many-body system. The relaxation is slower than for the single-particle bands and happens through Coulomb interaction [32], given in Eq. (6):

$$H_{\rm rel} = \sum_{k_{\rm phot},q} \int dq\, d\omega\, T(1,2)\rho(q,\omega)c_{bi}(k_F)c_i^\dagger(k_{\rm phot}), \quad (11)$$

where we annihilate the photohole by recombination with an electron from the Fermi surface. The energy momentum released in this decay process goes into a particle-hole collective density excitation, the eigenstate of the TLL, through electron-electron interaction $T_{1,2} \sim V_{\rm eff}(x)$. The last two annihilation-creation operators in Eq. (11) can be together called the *photodensity* $\rho_i(\vec{r}) \equiv c(k_F)c_i^\dagger(k_{\rm phot})$. Since the Hermite polynomial $H_0(r_\perp)$ is a symmetric Gaussian, then the overall symmetry of $\rho_i(r_\perp)$ is determined by a wave function of the $c_{A1,3}(k_F)$, i.e., $\psi_{A1,3}(\vec{r};k_{F1,3})$ is a wave function (at the Fermi level) of a matching band, see Fig. 5 for $|\psi_i(r_\perp)|$.

Contrary to the Fermi liquid, in TLL for each momenta we have four bosonic branches and the strength of each relaxation channel is proportional to an overlap integral between a photodensity $\rho_i(\vec{r})$ (defined above) and a given collective excitation of TLL. The amplitude of the process, when resolved among different bosonic modes, reads as

$$T(1=i,2=\nu) = \int dr_\perp V_{\rm eff}(\vec{r})\rho_\nu(\vec{r})\psi_i(\vec{r})\psi_{A1,3}(\vec{r};k_{F1,3}), \quad (12)$$

where $\rho_i(\vec{r}) = \psi_i(\vec{r})\psi_{A1,3}(\vec{r};k_{F1,3})$ and $\rho_\nu(\vec{r}) = \nabla\phi_\nu$. Different TLL modes have different symmetry with respect to the middle horizontal plane of the two-leg ladder: the total modes $\nabla\phi_{\rho+}$, $\nabla\phi_{\sigma+}$ describe in-phase oscillations of the densities of the two legs of the ladder while the transverse modes $\nabla\phi_{\rho-}$, $\nabla\phi_{\sigma-}$ describe antiphase oscillations. On the other hand, the difference between the two DFT bands is that one is symmetric (the bonding one $A3$ in [18,19] $NbSe_3$) and the other antisymmetric (antibonding one $A1$ in [18,19] $NbSe_3$) on the rung that links the two legs of the ladder. Hence, we can deduce that for (ω, k) emission point close to the$A3$ (bonding band) dispersion $\rho_i(\vec{r})$ is an electron-hole described as a wave with two legs oscillating in phase, while for (ω, k) close to the $A1$ (antibonding) band $\rho_i(\vec{r})$ is a hole's wave function with an extra π phase (or a minus sign) between the two legs of the ladder. The potential given by Eq. (5) is symmetric and, because small-q scattering dominates (see Fig. 3), does not allow to mix (ω, k) points. Then, overall change of sign of integrand implies that some amplitudes $T(1,2)$ in Eq. (12) are suppressed. For (ω, k) emission point close to the $A3$ (bonding band) relaxation into TLL eigenstates of the total holon and spinon modes is much more probable, while for (ω, k) emission point close to the $A1$ (antibonding band) relaxation into transverse holon and spinon modes is much more probable.

VII. DISCUSSION AND CONCLUSIONS

A. Comparison with experiment

We can now compare our results with a recent experiment [18,19] on $NbSe_3$. In Ref. [19] at each Fermi point *two* linear dispersions were detected, precisely as it was predicted in the previous section. For the inner (antibonding) band the two branches are distinguishable only when the dispersion approaches the Γ point of Brillouin zone since one is linear (charge) and one is parabolic (spin). For the bonding band Fermi point k_{F3}, we see two different velocities already at the Fermi level. We predict that the velocity of the spinon branch at k_{F3} (total spin mode $\sigma+$) should be equal to the velocities of the transverse modes visible at k_{F1}. This is despite the fact that DFT dispersions, the velocities extracted from DFT bands, are different by ≈15%–20%. The experiments observe these velocities to be equal. The holon branch visible at k_{F3} has been found in Eq. (10) to have velocity approximately 25% higher than other dispersions in good agreement with experiment [19]. It should be emphasized that our selection rule is less strict than the standard dipole-matrix selection rule as it essentially relies on the fact that $V_{\rm eff}(q)$ is strongly decaying with q and that there are no other states available close to E_F. As we reason in Appendix C, once the dispersion crosses the other states a recovery of $\rho+$ mode intensity in the antisymmetric band (e.g., $A1$ in $NbSe_3$) is permitted. Experimentally, it manifests as an emergence of a second, shifted Dirac cone (≈0.1 eV below the bottom of the $\rho-$ cone) with a velocity $v_{\rho+}$ substantially larger than V_F. Remarkably, this more subtle effect has been also observed in Refs. [18,19].

Other realizations. With small modifications, the result of this work can be also applied to systems that are recently under intense scrutiny: artificial 1D systems created (or self-organized) on a dielectric surface. Here, it has to be noted that our approach is complementary to the one derived in

Ref. [33] where they have modeled a single wire of a substantial cross section, i.e., a mesoscopic charge density with tenths or even hundreds of atoms in the cross section. Then, charge density can be approximated as a solution of a classical Poisson equation. However, such model, initially developed in a very different context and hence neglecting entire atomic and orbital physics, cannot be used as reliable approximation in a sub-nm domain when the atomistic physics plays a role. For instance, for domain walls on a surface of a topological insulator [34], where we know that the domain wall width covers only a few atoms, our microscopic approach can offer a much better approximation.

B. Validity of the TLL approximation

As we have already mentioned in Sec. II, the TLL description is valid provided our temperature and frequency range lies above any spectral gap of the system. What is missing in Eq. (1) are nonlinear cosine terms that are either due to exchange or backscattering processes. Although the precise form of these terms will vary depending which precise microscopic model needs to be taken, one of the most general expressions for the two-leg ladder with large t_r (so *not* for a double-chain problem coupled through V_r) has been in given in Ref. [28]. It reads as follows:

$$\begin{aligned} H^{NL}_{\text{int}(1)} = &-g_{1c}\int dr\,\cos(2\phi_{\sigma+})\cos(2\theta_{\rho-}) + g_{1a}\int dr\,\cos(2\phi_{\sigma+})\cos(2\theta_{\sigma-}) - g_{2c}\int dr\,\cos(2\theta_{\rho-})\cos(2\phi_{\sigma-}) \\ &+ g_{4a}\int dr\,\cos(2\phi_{\sigma-})\cos(2\theta_{\sigma-}) + g_{1}\int dr\,\cos(2\phi_{\sigma+})\cos(2\phi_{\sigma-}) \\ &+ g_{2}\int dr\,\sin(2\phi_{\sigma-})\sin(2\phi_{\sigma+}) + g_{\|c}\int dr\,\cos(2\theta_{\rho-})\cos(2\theta_{\sigma-}). \end{aligned} \tag{13}$$

We use the following notation: indices 1 to 4 refer to the standard *g-ology* processes for the left and right moving carriers, letters a to d correspond to similar processes, when the band's $j = o, \pi$ index is used instead of the left or right labels. We should emphasize here that we assume to be far away from any commensurate filling, where highly relevant umklapp and Peierls terms will likely open large gaps in the charge sector. The remaining nonlinear terms are usually tackled by means of renormalization group (RG) where the highest-energy degrees of freedom are gradually integrated out and we analyze towards which fixed point the system flows.

The interactions are originally defined in the band basis and then upon performing the $S[\pi/4]$ rotation to total-transverse basis we shall also have off-diagonal terms $\approx g_{oo} - g_{o\pi}$. To tackle these, alongside with the Fermi velocity difference $\Delta V_F = V_{Fb1} - V_{Fb3}$, we need to introduce renormalization group (RG) procedure that involves so far neglected backscattering terms. It can be shown Ref. [28] that for finite interband backscattering terms $\sim V_{o\pi}(2k_F)$, thanks to the fact that $K_{\rho+} \ll K_{\rho-}$, the band basis will relatively quickly flow towards the total-transverse basis while the Fermi velocities will flow to the average from both bands $(V_{Fb1} + V_{Fb3})/2$. Indeed, the value $\approx (V_{Fb1} + V_{Fb3})/2$ has been experimentally observed for $v^s_{1,3}$ in Ref. [19]. The terms $g_{1,2}$ describe the intraband backscattering, in total-transverse basis they are competing to lock spin field at different minima, so the RG flow away from the band basis makes it hard for these terms to open a gap.

It is also well known that for Hubbard-type models the above given perturbations alone lead to substantial gaps. However, for Coulomb-type models the gaps are predicted to be several orders of magnitude smaller, down to a value so small that will not be visible in most experiments. We want to discuss this difference in here. In the Hubbard model close to half-filling the gap opens first in the $\theta_{\rho-}$ mode which then drives the two-leg ladder to a superconducting order with a local d-wave symmetry, known as dSC phase (with overall three gapped modes). The underlying reason for that are substantial initial amplitudes of several nonlinear terms that contain $\cos 2\theta_{\rho-}$. These amplitudes are proportional to $V(2k_F)$ and inter band exchange. Our result, Fig. 3, is remarkable because of two reasons. Not only does it predict a finite value of interaction at $q \to 0$, but *at the same time* it decreases strongly with q. We see that screening proceeds in two stages: the approximation that we propose (RPA plus inter-TLL incoherent tunneling) is sufficient to cure the divergence, but at this level the forward scattering is still much more preferred than backward scattering. The hypothesis would be that one needs to invoke vertex corrections, for instance, some level of interladder coherence, to arrive in the regime where $V(2k_F) \approx V(q = 0)$. There is also a fundamental problem with interband exchange terms: these terms will be nonzero only if the lattice symmetry that permitted to define bonding and antibonding bands is broken. To be precise, since these are defined on the top of some DFT calculation, we need the correlation interaction that will break this symmetry. If it is the C_2 symmetry with respect to central axis of the ladder, then purely local Hubbard U on off-centered atom can break the symmetry, but a long range $V, J(q)$ that covers many atomic sites in several unit cells does not break this symmetry. Hence, this other component of the interband g_{1c}, g_{2c}, g_{1a} amplitudes is zero. Remarkably, in Sec. IV B, we have found $K_{\rho-} < 1$ and it has to stay like this because renormalization of K_ν is second-order effect proportional to g^2_ν which is extremely small in our case. For $K_{\rho-} < 1$ all terms in the sine-Gordon extension [28] of our TLL model $\sim \cos(2\theta_{\rho-})$ are irrelevant.

We can now analyze if the transition to the gapped phase can be driven by the spin sector alone. Finite exchange and $V(2k_F)$ processes allow for nonzero initial (UV) g_σ terms, which means that $K_{\sigma+}$ may deviate from one. However, provided spin-rotational symmetry is preserved, the flow of this mode would proceed towards $K^*_{\sigma+} = 1$ (provided it is not disturbed by strong $\theta_{\rho-}$ RG flow). As for the $\sigma-$ sector we notice the presence of $\cos(\phi_{2\sigma-})$ and $\cos(\theta_{2\sigma-})$ terms. The two

fields are canonically conjugated, so they cannot be gapped at the same time. A characteristic aspect of Coulomb-type interactions is that, contrary to Hubbard-type interactions, it involves also the interaction of electrons with the same spin $g_{\|c}$. This amplitude is nonzero already in the UV limit, hence, various cosines compensate each other. This situation persists throughout RG flow. The case $K_{\sigma-}=1$, predicted in Sec. IV B, is marginal with cosines of neither field relevant. To have $K_{\sigma-}\neq 1$, in the UV limit, one has to have a model with either exchange or spin-rotational symmetry breaking that depends on the band index. We conclude that even in the more generalized sine-Gordon two-leg ladder model, the competition between $\cos(\phi_{2\sigma-})$ and $\cos(\theta_{2\sigma-})$ remains tied. The competition between $\cos(\phi_{\sigma-})$ and $\cos(\theta_{\sigma-})$ terms, that can be ultimately resolved only through refermionization [13], will impede a swift spectral gap opening so the TLL phase is not destabilized. The conclusion of Ref. [13], about the $\sigma-$ gaps of order 10^{-4} K will then remain valid as long as we are not facing the system with strong site-dependent spin-orbit coupling or band-dependent strong Rashba interactions. For any temperature greater than that the system will effectively behave like the TLL and our theory applies.

The above given arguments for the validity of TLL description can only be broken by the presence of an additional strongly relevant backscattering term in the Hamiltonian. This may be, for instance, charge confinement leading to Coulomb blockade, as proposed first in Ref. [35], but also other schemes although much milder are also possible, for instance, in nanotubes due to curvature-induced spin-orbit coupling [36].

C. Conclusions

In conclusion, we have given a closed analytic expression (6) for the density-density interactions in quasi-1D materials. This generalizes the previously known formula [13] for a homogeneous charge distribution on the circumference of a nanotube to a more arbitrary charge distribution. This extension can cover most experimental realizations. In particular, we showed that, for the case of long-range interactions that obey the crystal lattice symmetries, the distribution of charge density is a sufficient information to give the TLL parameters and hence all correlation functions of the system. Furthermore, in Eq. (7) we have introduced screening from all other 1D systems in the quasi-1D material. This allows to obtain a finite value of TLL holon velocity even in a thermodynamic limit. It is an improvement with respect to numerous studies in the past where a mesoscopic charging energy had to be introduced artificially to avoid a divergence of holon velocity. Our procedure provides the TLL parameters from input parameters known from DFT calculations, such as the orbital's shape and a strength of local interaction (effective Hubbard U, e.g., from cRPA). Furthermore, we showed that a careful averaging [Eqs. (9) and (10)] needs to be used to obtain a quantity that can be compared with an outcome of ARPES experiment. We also showed that our theory can predict, from Eq. (12), relative intensities obtained in ARPES for different bosonic branches. With these results we validate our theory by comparing its findings to an ARPES result [18,19] on recently studied material $NbSe_3$. Hence, we have completed a link between the *ab initio* DFT results and experimental ARPES measurement. Our reasoning can serve as a benchmark for future ARPES studies of similar quasi-1D compounds.

ACKNOWLEDGMENTS

I would like to sincerely thank T. Giamarchi, M. Grioni, S. Pons, and M. A. Valbuena for numerous discussions that inspired this study and, in particular, E. Canadell for sharing his vast knowledge on quasi-1D materials.

APPENDIX A: INTERACTIONS IN THE SPECIFIC CASE OF $NbSe_3$

The bands' resolved interaction amplitudes g_{mn} will depend on a specific system under consideration. In the particular case of $NbSe_3$ the bonding orbital, see Fig. 5 (left panel), is more spread (larger angle ϕ), thinner and closer to the center (smaller R and d) which results in $V^{\pi\pi}\leqslant V^{oo}$. This is compensated by the Fermi velocity difference $V_{F\pi}<V_{Fo}$ so $g_{oo}\approx g_{\pi\pi}$. The interband terms are more complicated to analyze. We assume that the product of the two densities is intermediate but also less homogeneous (larger ζ), see Fig. 5 (right panel), which results in larger $V_{o\pi}$ (see Fig. 2). However, the interband Hartree interaction is also reduced by a factor $V_{2o\pi}=J_0((k_{Fo}-k_{F\pi})a)V_{oo}$ where $J_0(k)$ is a Bessel function of the first kind. This is arising from computing an overlap between two waves of slightly different periodicity: one takes two phase-shifted waves and integrates over the phase shift. Furthermore, the $J_{o\pi}=0$, a result which can be obtained directly by noticing that integrand in an analog of Eq. (3) (main text) has two functions of opposite parity or, if we treat band index as pseudospin variable, then the interband scattering is an antiparallel (pseudo)spin process where particles are distinguishable so quantum exchange is zero. Treating the band index as a (pseudospin) quantum number is admissible only for a $t_\perp$ hybridization coupled ladders provided $t_\perp$ is large enough such that many-body terms do not perturb bands substantially. Overall, we find $g_{oo}/g_{o\pi}\approx 1.12$. To parametrize interactions in Eq. (5) (main text), for the case of Nb atom, we use the following cRPA value [37] $U=2.8$ eV which, with $N=4$, give $\bar{U}=0.7$ eV while for the exchange $J=0.4$ eV.

As it was proven in the main text (see Fig. 3), weakly screened interaction retains predominantly long-range character and then the three modes ($\sigma\pm$ and $\rho-$) have velocities that are very close to the average Fermi velocity [average from both bands $(V_{Fb1}+V_{Fb3})/2$ where $V_{Fb1,3}$ are known from DFT] and so these dispersions are rather close to each other, while interactions affect only the total charge-mode ($\rho+$) velocity which is noticeably larger.

APPENDIX B: FERMIONIC MODEL

The simplest, minimal lattice model that can capture the two-leg ladder class of Hamiltonians is given by the following tight-binding Hamiltonian:

$$\begin{aligned}H_{\text{example}}=&\sum_{i,j}[t_b(c_i^\dagger(j,\pm R/2)c_{i+1}(j,\pm R/2)+\text{H.c.})\\&+t_r(c_i^\dagger(j,+R/2)c_i(j,-R/2)+\text{H.c.})]\\&+\sum_{i,j}t_\perp(c_i^\dagger(j)c_i(j+1)+\text{H.c.}),\end{aligned}\tag{B1}$$

where index i counts the sites along the conducting b axis (along the column in Fig. 4) while the j index is perpendicular to it. The t_r is hopping on the rung of the two-leg ladder, between the two subunits that build a column. The hopping $t_\perp \ll t_b, t_r$ is the hopping between the columns, which is not accounted for in Eq. (1) but enters in Sec. IV. The t_r parametrizes the split between so-called bonding ("o") and antibonding ("π") bands shown on the inset in Fig. 4. Each subunit of the column may consist of several atomic sites; this is a rather usual situation, for instance, in $NbSe_3$ each subunit consists of two biprisms (two Nb and six Se atoms). Then, each atomic site has some onsite energy, e.g.,E_{SeII}, and in the simplest case the ratio of these energies and eigenenergies of Eq. (B1) determine local charge densities whose distribution may well be different for the two bands. Also, Eq. (B1) is the simplest model while realistic description dedicated to a real material requires several hopping paths, several tight-binding parameters. Also, these parameters may be renormalized by higher-order interaction processes (acquire self-energy) and become momentum dependent. For the purposes of this paper, we identified that the key parameter that shall determine low-energy physics is the charge distribution $\bar{\rho}(\vec{r})$ irrespective of underlying microscopic Hamiltonian.

In order to get $K_\nu \neq 1$ in Eq. (1), one needs to supplement the kinetic energy part of Hamiltonian [e.g., Eq. (B1)] with interactions given by Eq. (2). Assuming that Eq. (B1) represents a result of some mean-field theory (like DFT) we develop our description around this saddle point. This means that at the shortest distances the interactions are screened by high-energy excitations capable of creating electron-hole pairs from bands and orbitals that support 3D propagation. That is why the $\Lambda_U V$ is an essential part of the theory, and in particular it can serve to determine the $\bar{U}$ as described in the main text.

APPENDIX C: DETAILS OF COMPARISON WITH REFS. [17,18]

The reasoning that led us to conjecture about the parabolic and Dirac nature of spin and charge dispersions relies on an exact analytic solution for a single-chain Hubbard model [38]. The numerical results for extended Hubbard models [39] suggest that there is no qualitative modification of this spectrum as the range of interaction is changed, like in U-V-W models. Hence, if we assume that there is no high-energy phase transition induced by changing range of the interaction, then the two charge modes shall cross at the Γ points (forming structures that each resemble a Dirac point with constant velocities) while the two spin modes shall have parabolic behavior [hence, $v_{\sigma\pm}(q_{||} \to \Gamma) \to 0$] close to the Γ point. This assumption should hold provided that the hopping between chains is not extremely strong (and on-rung interaction is not large), i.e., the on-chain physics dominates the on-rung physics. In that latter case, the physics of relative charge mode can be written as a pseudospin variable and the crossover to Coulomb interaction case can be complicated. However, this is not the problem of our study where $t_\perp < t_b$ and $V_\perp < V_{\mathrm{Coul}}$.

Concerning the relative intensities of the modes at higher energies, the situation becomes even more complex if the TLL holon dispersion crosses a single-particle band as it happens, e.g., with band $C2$ in $NbSe_3$ [19]. Then, the photohole may relax much faster into these single-particle states especially in the vicinity of the crossing point. For a simple set of master rate equations $\dot{n}_{C2} = r_{C2}\rho_i(t); \dot{n}_{\rho+} = r_{\rho+}\rho_i(t)$, we see that when the rate of transition into single-particle states is higher (which is to be expected since here only one fermionic instead of entangled bosonic states are involved) $r_{C2} \gg r_{\rho+}$ then asymptotically the system moves to a situation with most excitations in the auxiliary band C2. This shall manifest in the experiment since at the crossing with the dispersion of the single-electron $b2$ band we expect that $\psi_i(\vec{r})$ will sink out into this auxiliary dispersion so the intensity of the bosonic branches will be diminished.

When energy of the photohole is larger than that of the electron's bound within the band $C2$, then a two-stage process is possible: in the first stage a single particle from the $C2$ falls onto a photohole state and later the $b2$ hole relaxes onto Fermi level, producing the final bosonic excitation $1_i \to 1_{b2+\nu} \to 2_\nu$. This is a higher-order process with two *intermediate e-h* involved, but it may be favored by the faster $C2$ relaxation rate. Then, the selection rule described in the main text Sec. VI does not apply any more, instead, the amplitude is proportional to the $T(1_i, 1_{b2+\nu}, 2_\nu)$. Furthermore, $\rho_i(\vec{r})$ is created for binding energies above 0.3 eV; then, following the same argument we expect that it shall have bigger overlap with total holon modes. Hence, the intensity should increase again and one should notice an increase of holon velocity for the $A1$ band. This is what has been reported in the experiment [19].

APPENDIX D: INTERACTION COUPLED LADDER

The results presented in this work are for a ladder coupled through single-particle hybridization on the rung t_r and inter-ladder Coulomb couplings $V_\perp$. However, our method can be also applied to an interaction coupled ladder, the double-chain problem with $V_r \gg t_r$. Here each 1D column would have been built of two *identical* 1D clumps of charge (along the chain), so for the entire ladder the symmetry is lowered down to $C_2(\vec{b}), S_2(\vec{b})$. Crucially, in the interaction V_r coupled ladder the t_r has to be neglected (otherwise it may produce dangerously relevant cosine and chemical potential terms) and both $K_{\rho\pm}$ are determined through a split of the single leg K_ρ by $\sim V_r$ so we shall have two modes that are far from $K_\nu = 1$ and so there are two modes that enter Eqs. (9) and (10). This case is open for further studies, possibly when an appropriate experimental realization occurs.

[1] F. D. M. Haldane, "Luttinger liquid theory" of one-dimensional quantum fluids. I. Properties of the Luttinger model and their extension to the general 1D interacting spinless Fermi gas, J. Phys. C: Solid Stae Phys. **14**, 2585 (1981).

[2] R. Claessen, G.-H. Gweon, F. Reinert, J. Allen, W. Ellis, Z. Shen, C. Olson, L. Schneemeyer, and F. Lévy, Angle-resolved photoemission of quasi-one-dimensional metals: Evidence for luttinger liquid behavior, J. Electron Spectrosc. Relat. Phenom. **76**, 121 (1995), Proceedings of the Sixth International Conference on Electron Spectroscopy.

[3] L. Dudy, J. D. Denlinger, J. W. Allen, F. Wang, J. He, D. Hitchcock, A. Sekiyama, and S. Suga, Photoemission spectroscopy and the unusually robust one-dimensional physics of lithium purple bronze, J. Phys.: Condens. Matter **25**, 014007 (2012).

[4] G.-H. Gweon, J. W. Allen, and J. D. Denlinger, Generalized spectral signatures of electron fractionalization in quasi-one- and two-dimensional molybdenum bronzes and superconducting cuprates, Phys. Rev. B **68**, 195117 (2003).

[5] Y. Ma, H. C. Diaz, J. Avila, C. Chen, V. Kalappattil, R. Das, M.-H. Phan, T. Čadež, J. M. P. Carmelo, M. C. Asensio *et al.*, Angle resolved photoemission spectroscopy reveals spin charge separation in metallic $MoSe_2$ grain boundary, Nat. Commun. **8**, 14231 (2017).

[6] B. Kim, H. Koh, E. Rotenberg, S. Oh, H. Eisaki, N. Motoyama, S. Uchida, T. Tohyama, S. Maekawa, Z. Shen, and C. Kim, Distinct spinon and holon dispersions in photoemission spectral functions from one-dimensional $SrCuO_2$, Nat. Phys. **2**, 397 (2006).

[7] D. Bounoua, R. Saint-Martin, J. Dai, T. Rödel, S. Sengupta, E. Frantzeskakis, F. Bertran, P. Lefevre, F. Fortuna, A. F. Santander-Syro, and L. Pinsard-Gaudart, Angle resolved photoemission spectroscopy study of the spin-charge separation in the strongly correlated cuprates $SrCuO_2$ and Sr_2CuO_3 with S=0 impurities, J. Electron Spectrosc. Relat. Phenom. **225**, 49 (2018).

[8] T. Giamarchi, *Quantum Physics in One Dimension* (Oxford University Press, Oxford, 2004).

[9] U. Schollwöck, The density-matrix renormalization group, Rev. Mod. Phys. **77**, 259 (2005).

[10] S. Ejima, F. Gebhard, and S. Nishimoto, Tomonaga-Luttinger parameters and spin excitations in the dimerized extended Hubbard model, Phys. Rev. B **74**, 245110 (2006).

[11] S. Ejima, F. Gebhard, and S. Nishimoto, Tomonaga-Luttinger parameters for doped Mott insulators, Europhys. Lett. **70**, 492 (2005).

[12] S. J. van Tongeren, Introduction to the thermodynamic Bethe ansatz, J. Phys. A: Math. Theor. **49**, 323005 (2016).

[13] R. Egger and A. O. Gogolin, Correlated transport and non-Fermi-liquid behavior in single-wall carbon nanotubes, Eur. Phys. J. B **3**, 281 (1998).

[14] Z. S. Popović and S. Satpathy, Density-functional study of the Luttinger liquid behavior of the lithium molybdenum purple bronze $Li_{0.9}Mo_6O_{17}$, Phys. Rev. B **74**, 045117 (2006).

[15] E. Canadell, I. E. I. Rachidi, J. P. Pouget, P. Gressier, A. Meerschaut, J. Rouxel, D. Jung, M. Evain, and M. H. Whangbo, Comparison of the electronic structures of layered transition-metal trichalcogenides thallium triselenide, thallium trisulfide and niobium triselenide, Inorg. Chem. **29**, 1401 (1990).

[16] R. M. Konik and P. Fendley, Haldane-gapped spin chains as Luttinger liquids: Correlation functions at finite field, Phys. Rev. B **66**, 144416 (2002).

[17] R. Konik, F. Lesage, A. W. W. Ludwig, and H. Saleur, Two-leg ladders and carbon nanotubes: Exact properties at finite doping, Phys. Rev. B **61**, 4983 (2000).

[18] M. A. Valbuena, P. Chudzinski, S. Pons, S. Conejeros, P. Alemany, E. Canadell, H. Berger, E. Frantzeskakis, J. Avila, M. C. Asensio, T. Giamarchi, and M. Grioni, Polarization dependence of angle-resolved photoemission with submicron spatial resolution reveals emerging one-dimensionality of electrons in $NbSe_3$, Phys. Rev. B **99**, 075118 (2019).

[19] M. A. Valbuena, P. Chudzinski, S. Pons, S. Conejeros, P. Alemany, E. Canadell, H. Berger, E. Frantzeskakis, J. Avila, M. C. Asensio, T. Giamarchi, and M. Grioni, Emerging one-dimensionality from self-organization of electrons in $NbSe_3$, arXiv:1612.04712.

[20] J. Hager, R. Matzdorf, J. He, R. Jin, D. Mandrus, M. A. Cazalilla, and E. W. Plummer, Non-Fermi-Liquid Behavior in Quasi-One-Dimensional $Li_{0.9}Mo_6O_{17}$, Phys. Rev. Lett. **95**, 186402 (2005).

[21] A. A. Nersesyan and A. M. Tsvelik, Coulomb blockade regime of a single-wall carbon nanotube, Phys. Rev. B **68**, 235419 (2003).

[22] M. Tsuchiizu, P. Donohue, Y. Suzumura, and T. Giamarchi, Commensurate-incommensurate transition in two-coupled chains of nearly half-filled electrons, Eur. Phys. J. B **19**, 185 (2001).

[23] P. Chudzinski, T. Jarlborg, and T. Giamarchi, Luttinger-liquid theory of purple bronze $Li_{0.9}Mo_6O_{17}$ in the charge regime, Phys. Rev. B **86**, 075147 (2012).

[24] A. Iucci, G. A. Fiete, and T. Giamarchi, Fourier transform of the $2k_F$ Luttinger liquid density correlation function with different spin and charge velocities, Phys. Rev. B **75**, 205116 (2007).

[25] F. H. L. Essler and A. M. Tsvelik, Finite Temperature Spectral Function of Mott Insulators and Charge Density Wave States, Phys. Rev. Lett. **90**, 126401 (2003).

[26] P. Chudzinski, Why it is so hard to detect Luttinger liquids in angle resolved photo-emission spectroscopy? J. Phys.: Condens. Matter **31**, 105601 (2019).

[27] A. O. Gogolin, A. A. Nersesyan, and A. M. Tsvelik, *Bosonization and Strongly Correlated Systems* (Cambridge University Press, Cambridge, 1999).

[28] P. Chudzinski, M. Gabay, and T. Giamarchi, Orbital current patterns in doped two-leg Cu-O Hubbard ladders, Phys. Rev. B **78**, 075124 (2008).

[29] H. J. Schulz, Long-range Coulomb interactions in quasi-one-dimensional conductors, J. Phys. C: Solid State Phys. **16**, 6769 (1983).

[30] M.A. Valbuena (private communication).

[31] D. Mou, R. M. Konik, A. M. Tsvelik, I. Zaliznyak, and X. Zhou, Charge-density wave and one-dimensional electronic spectra in blue bronze: Incoherent solitons and spin-charge separation, Phys. Rev. B **89**, 201116(R) (2014).

[32] T. Karzig, L. I. Glazman, and F. von Oppen, Energy Relaxation and Thermalization of Hot Electrons in Quantum Wires, Phys. Rev. Lett. **105**, 226407 (2010).

[33] J. C. Y. Teo and C. L. Kane, Critical behavior of a point contact in a quantum spin Hall insulator, Phys. Rev. B **79**, 235321 (2009).

[34] R. Stahler, F. Reis, T. Maller, T. Helbig, T. Schwemmer, R. Thomale, J. Schafer, and R. Claessen, Tomonaga-Luttinger liquid in the edge channels of a quantum spin Hall insulator, Nat. Phys. **16**, 47 (2020).

[35] L. S. Levitov and A. M. Tsvelik, Narrow-Gap Luttinger Liquid in Carbon Nanotubes, Phys. Rev. Lett. **90**, 016401 (2003).

[36] P. Chudzinski, Spin-orbit coupling and proximity effects in metallic carbon nanotubes, Phys. Rev. B **92**, 115147 (2015).

[37] E. Şaşıoğlu, C. Friedrich, and S. Blügel, Effective Coulomb interaction in transition metals from constrained random-phase approximation, Phys. Rev. B **83**, 121101(R) (2011).

[38] E. H. Lieb and F. Y. Wu, The one-dimensional Hubbard model: A reminiscence, Phys. A **321**, 1 (2003).

[39] F. Mila and X. Zotos, Phase diagram of the one-dimensional extended Hubbard model at quarter-filling, EPL **24**, 133 (1993).